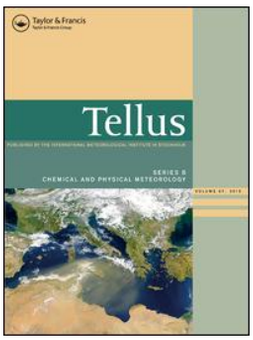

Tellus B: Chemical and Physical Meteorology

ISSN: (Print) 1600-0889 (Online) Journal homepage: http://www.tandfonline.com/loi/zelb20

Regional simulation of anthropogenic sulfur over East Asia and its sensitivity to model parameters

Yun Qian, Filippo Giorgi, Yan Huang, William Chameides & Chao Luo

To cite this article: Yun Qian, Filippo Giorgi, Yan Huang, William Chameides & Chao Luo (2001) Regional simulation of anthropogenic sulfur over East Asia and its sensitivity to model parameters, Tellus B: Chemical and Physical Meteorology, 53:2, 171-191, DOI: 10.3402/tellusb.v53i2.16573

To link to this article: http://dx.doi.org/10.3402/tellusb.v53i2.16573

Tellus (2001), 53B, 171–191
Printed in UK. All rights reserved

TELLUS
ISSN 0280–6509

Regional simulation of anthropogenic sulfur over East Asia and its sensitivity to model parameters

By YUN QIAN[1,3], FILIPPO GIORGI[1,*], YAN HUANG[2], WILLIAM CHAMEIDES[2] and CHAO LUO[2], [1]*Abdus Salam International Centre for Theoretical Physics, Trieste, Italy;* [2]*Georgia Institute of Technology, Atlanta, Georgia, USA;* [3]*START Regional Center for TEA, IAP/CAS, Beijing, China*

(Manuscript received 16 February 2000; in final form 29 September 2000)

ABSTRACT

We discuss a series of simulations of anthropogenic sulfur over East Asia with a SO_2/SO_4^{2-} chemistry-transport model driven in on-line mode by a regional climate model. Sensitivity to OH and H_2O_2 concentration, cloud parameters, SO_2 dry deposition and emission strength is analyzed and the different components of the sulfur budget are examined. The SO_2 and SO_4^{2-} column burdens show pronounced variability at temporal scales from seasonal to synoptic and sub-daily, with SO_2 and SO_4^{2-} behaving differently due to the interplay of chemical conversion, removal and transport processes. Both SO_2 and SO_4^{2-} show marked spatial variability, with emission being the dominant term in regulating the SO_2 spatial distribution. The atmospheric SO_2 and SO_4^{2-} amounts show close to a linear response to surface emission. Aqueous phase $SO_2 \rightarrow SO_4^{2-}$ conversion and wet removal are the primary factors that regulate the SO_4^{2-} amounts, with dry deposition and gas phase $SO_2 \rightarrow SO_4^{2-}$ conversion being of secondary importance. Aqueous phase conversion and dry deposition are the dominant loss mechanisms for SO_2. The model shows low sensitivity to variations in OH, H_2O_2, and cloud parameters, while the sensitivity to prescribed dry deposition velocity is more pronounced. Overall, our results are in line with previous modeling studies and with very limited available observations.

1. Introduction

It is by now recognized that anthropogenic emissions of pollutants due to urban, industrial and agricultural activities can have significant climatic and environmental effects, especially at the regional scale (IPCC, 1996). This issue is particularly important for highly industrialized regions, such as the continental U. S. and Europe, and rapidly developing ones, such as East and South Asia, where pollutant emission is already very high or is expected to increase rapidly in the coming decades.

One of the pollutants that has drawn most attention is sulfur dioxide (SO_2), which is emitted as a gaseous product of combustion processes, for example fossil fuel combustion (Rodhe, 1999). Once released into the atmosphere, SO_2 is oxidized to eventually generate sulfate aerosol particles (SO_4^{2-}). These particles scatter solar radiation ("direct effect") and can act as cloud condensation nuclei, thereby modifying the cloud microphysical and optical properties ("indirect effects"). Inclusion of sulfate aerosol effects in climate simulations has provided evidence of significant climatic forcing by aerosol particles (IPCC, 1996).

The $SO_2 \rightarrow SO_4^{2-}$ oxidation process involves complex chemical mechanisms both in the gas and aqueous (cloud) phase (Chameides, 1984). At present, it is not feasible to incorporate these full mechanisms within complex climate models, so

* Corresponding author.
email: giorgi@ictp.trieste.it

that a number of simplified sulfur chemistry schemes including only a few tracers have been developed for climate studies (Langner and Rodhe, 1991; Pham et al., 1995; Chin et al., 1996; Kasibhatla et al., 1997; Feichter et al., 1996; Lohmann et al., 1999; Barth et al., 2000; Rasch et al., 2000). Most of these studies have employed global models with relatively coarse resolution. On the other hand, the recent development of regional climate models (Giorgi and Mearns, 1991, 1999; Giorgi, 1995) and the regional nature of anthropogenic sulfur emissions make the study of regional effects of sulfur compounds suitable for the use of regional modeling systems.

One of the geographical areas for which the issue of environmental effects of anthropogenic pollutants is especially relevant is East Asia, currently one of the most rapidly developing regions of the globe. Pollutant emission over East Asia has been continuously and rapidly increasing over the last decades, and is expected to continue to increase for the coming ones (Streets and Waldhoff, 1999). Both observational and modeling studies have suggested that gaseous and particulate compounds might affect regional climate, agricultural productivity and local ecosystems (Qian and Fu, 1997; Zhou et al., 1998; Qian and Giorgi, 1999; Chameides et al., 1999), and substantial modeling work has addressed the problem of acid deposition and inter-regional transport (Ichikawa and Fujita, 1995; Huang et al., 1995; Wang et al., 1996). Recently, an international project has been developed, called CHINA-MAP, aimed at elucidating mechanisms of interaction among anthropogenic activities, climate and agriculture for East Asia (Chameides, 1995). The central modeling tool for this project is a regional climate model, the RegCM described by Giorgi et al. (1993a, b; 1999) and Giorgi and Shields (1999), coupled to a hierarchy of chemistry-transport models.

As a first step towards coupling of regional chemistry, aerosol and climate models, Qian and Giorgi (1999) interactively coupled the RegCM to a first generation SO_4^{2-} model including source, transport, removal and radiative processes, but no chemical mechanisms. Their study was aimed at investigating the interactions between SO_4^{2-}, radiative forcing and regional climate. In the present paper we extend the work of Qian and Giorgi (1999) to examine the behavior of a second generation sulfur chemistry model incorporated within the RegCM framework. The model follows the approach of Kasibhatla et al. (1997). It includes both SO_2 and SO_4^{2-} as tracers and, along with source, transport and removal terms, a chemical mechanism of transformation from SO_2 to SO_4^{2-}. This is conceptually the simplest model that can explicitly account for $SO_2 \rightarrow SO_4^{2-}$ oxidation mechanisms, and it is expected to provide the basis for a series of regional climate experiments within the framework of the CHINA-MAP program.

With these premises, the primary goals of our work can be summarized as follows:

(1) To investigate the behavior of anthropogenic SO_2 and SO_4^{2-} over East Asia at a range of temporal and spatial scales, and to examine the relative role of emission, meteorological fields, chemical and removal mechanisms in regulating this behavior. Our analysis is limited to the sulfur cycle, and no aerosol radiative forcing on climate is included in the experiments. Also, we limit our study to sulfur of anthropogenic origin without accounting for the contribution of natural sources.

(2) The SO_2/SO_4^{2-} model adopts some simplifying assumptions in different chemical and cloud processes. A goal of this study is to evaluate the sensitivity of the model to these assumptions. This can also help to identify a suitable level of model complexity for use in regional sulfur chemistry-climate interaction studies.

Section 2 first describes model and experiment design. We then analyze results from our sensitivity experiments in Section 3 and present concluding remarks in Section 4.

2. Model and experiment design

2.1. Regional climate model

In this study, we use the version of RegCM originally developed by Giorgi et al. (1993a, b) with the augmentations of Giorgi and Shields (1999) and Giorgi et al. (1999). The RegCM, based on the NCAR/Pennsylvania State University mesoscale models MM4 and MM5, is a primitive equation, hydrostatic, grid point limited area model, with σ-pressure vertical coordinate. Surface processes are represented via the Biosphere–Atmosphere Transfer Scheme (Dickinson et al., 1993) and boundary layer phys-

ics is formulated following the non-local scheme of Holtslag et al. (1990). Resolvable scale precipitation is represented via the simplified explicit scheme described by Giorgi and Marinucci (1996) and Giorgi and Shields (1999), while the Kuo-type scheme of Anthes (1977) (in the simplified form described by Anthes et al., 1987) is used in our simulation to represent convective precipitation. Radiative transfer is described using the radiation package of the NCAR Community Climate Model, version CCM3 (Kiehl et al., 1996).

2.2.. *Sulfur model*

Our tracer model follows Kasibhatla et al. (1997). Two prognostic equations are solved for the mixing ratio (χ) of SO_2 and SO_4^{2-}

$$\frac{\partial \chi^{SO_2}}{\partial t} = -\bar{V}\nabla\chi^{SO_2} + F_H^{SO_2} + F_V^{SO_2} + T_{cum}^{SO_2} + S_r^{SO_2} - R_{w,ls}^{SO_2} - R_{w,cum}^{SO_2} - D_{dry}^{SO_2} - C_{SO_2\rightarrow SO_4^{2-}}, \quad (1)$$

$$\frac{\partial \chi^{SO_4^{2-}}}{\partial t} = -\bar{V}\nabla\chi^{SO_4^{2-}} + F_H^{SO_4^{2-}} + F_V^{SO_4^{2-}} + T_{cum}^{SO_4^{2-}} + S_r^{SO_4^{2-}} - R_{w,ls}^{SO_4^{2-}} - R_{w,cum}^{SO_4^{2-}} - D_{dry}^{SO_4^{2-}} - C_{SO_2\rightarrow SO_4^{2-}}, \quad (2)$$

The first term on the r.h.s. of eqs. (1) and (2) represents horizontal and vertical advection, F_H, F_V are horizontal and vertical turbulent diffusion, T_{cum} is vertical transport by cumulus clouds, S_r is a source term, $R_{w,ls}$, $R_{w,cum}$ are wet removal terms by resolvable scale and convective precipitation, respectively, D_{dry} is dry deposition, and $C_{SO_2\rightarrow SO_4^{2-}}$ is the $SO_2\rightarrow SO_4^{2-}$ chemical conversion term including both the gas phase and aqueous phase pathways.

All the advection and diffusion terms are the same as used in the MM5 for cloud water mixing ratio (Grell et al., 1993; Qian and Giorgi, 1999). For vertical transport by cumulus clouds it is assumed that when cumulus convection is activated the tracer becomes well mixed (constant mixing ratio) between the surface and the top of the cumulus cloud layer (Kasibhatla, pers. comm., Qian and Giorgi, 1999).

The parameterization of wet removal is based on the schemes of Giorgi and Chameides (1986) and Giorgi (1989). At the resolvable scale the model explicitly calculates cloud water content via the simplified explicit moisture scheme of Giorgi and Marinucci (1996) and Giorgi and Shields (1999). This consists of a prognostic equation for cloud water mixing ratio including transport, condensation, evaporation and a Kessler-type bulk autoconversion term that converts cloud water to rain water (see also Qian and Giorgi, 1999). Rain water is then immediately precipitated out. When resolvable scale precipitation occurs, it is assumed that the amount of tracer removed during the time step Δt is given by

$$R_{w,ls} = \chi f_{sol}(\chi)\frac{[1-\exp(-\Delta t/\tau_{w,ls})]}{\Delta t}, \quad (3)$$

where $f_{sol}(\chi)$ is the fraction of tracer dissolved into cloud water. For SO_4^{2-} this is assumed to be equal to 1, while for SO_2 it is given by the equilibrium dissolution value, which explicitly depends on the liquid water content (Chameides, 1984). $\tau_{w,ls}$ is a removal time for cloud water given by the cloud water mixing ratio divided by the conversion rate of cloud water to rain water (Qian and Giorgi, 1999). The values of $\tau_{w,ls}$ are highly variable since they depend on the cloud water content, but are generally of the order of several hours within large scale clouds. For resolvable scale wet removal we assume that the entire grid box is engulfed by the cloud.

A similar expression is used for cumulus cloud removal

$$R_{w,cum} = \chi f_{cum} f_{sol}(\chi)\frac{[1-\exp(-\Delta t/\tau_{w,cum})]}{\Delta t}, \quad (4)$$

where f_{cum} is the fraction of grid box occupied by cumulus convection and $\tau_{w,cum}$ is a removal time for cumulus cloud water assumed to be of the order of the lifetime of a cumulus cloud, i.e., $\sim$20 min. Following Giorgi and Chameides (1986), we adopt a value of $f_{cum} = 0.3$.

Below-cloud scavenging of SO_2 is included following the parameterization of Levine and Schwartz (1982), and dry deposition is parameterized using a constant deposition velocity (v_{dep}). The SO_4^{2-} deposition velocity has a value of 0.2 cm s^{-1} (Langner and Rodhe, 1991). For SO_2, different values of v_{dep} are tested, since a wide range of values have been used in the literature. In the base experiments we use values consistent with Luo et al. (2000), i.e., 0.8 cm s^{-1} over land and 0.4 cm s^{-1} over ocean, which are based on the estimates of Warnek (1988). Other studies,

however, have employed larger v_{dep} values over ocean than over land (Langner and Rodhe, 1991; Chin et al., 1996). Based on these studies, we completed two sensitivity experiments in which $v_{dep} = 0.8$ cm s^{-1} over ocean and 0.4 cm s^{-1} over land. The deposition velocity operates on the average concentration of the bottom model layer, which has a depth of about 40–45 m.

The conversion of SO_2 to SO_4^{2-} follows two oxidation pathways, one in the gas phase and one in the aqueous phase. The gas phase oxidation pathway is initiated by the reaction of SO_2 with OH, and thus depends on the OH concentration and the reaction rate coefficient. In our simulations, the rate coefficient is from DeMore et al. (1994) and includes an explicit dependence on temperature. The concentration of OH is taken from the regional simulation of Luo et al. (2000) who used the meteorological fields calculated by the RegCM to run a full chemistry-transport model (the Regional Acid Deposition Model, or RADM) for our domain and simulation period. For our experiments we had available monthly averaged values of spatially varying three-dimensional OH fields.

Fig. 1a shows examples of monthly averaged vertical profiles of OH concentration for July and November calculated by RADM and averaged over the model domain. A comparison of simulated OH with observations at 4 Chinese sites is discussed by Luo et al (2000). The basic spatial and temporal characteristics of OH show the following features: A significant latitudinal variation, with OH concentration decreasing with latitude; small longitudinal and vertical variation (Fig. 1a); pronounced diurnal cycle, with negligible nighttime concentrations; significant seasonal change (Fig. 1a).

Conversion of SO_2 to SO_4^{2-} in aqueous phase takes place via dissolution of SO_2 in cloud liquid water to form HSO_3^- and SO_3^{2} ions and subsequent oxidation of these ions by H_2O_2 and O_3. The reaction involving H_2O_2 is largely dominant at pH levels below 5 (Kasibhatla et al., 1997), which prevail over most of central, southern and eastern China where the highest sulfur concentration are located (Qian and Fu, 1998). In addition, previous work has indicated that reaction with O_3 only accounts for 10% of the SO_2 oxidation (Rasch et al., 2000). Therefore, we neglect oxidation by O_3, and following Kasibhatla et al. (1997), we assume no mass transport limitations in the conversion of SO_2 to SO_4^{2-} in cloud water. As a result, the amount of dissolved SO_2 converted to SO_4^{2-} is limited only by the available gas phase concentration of H_2O_2. Spatially varying three-

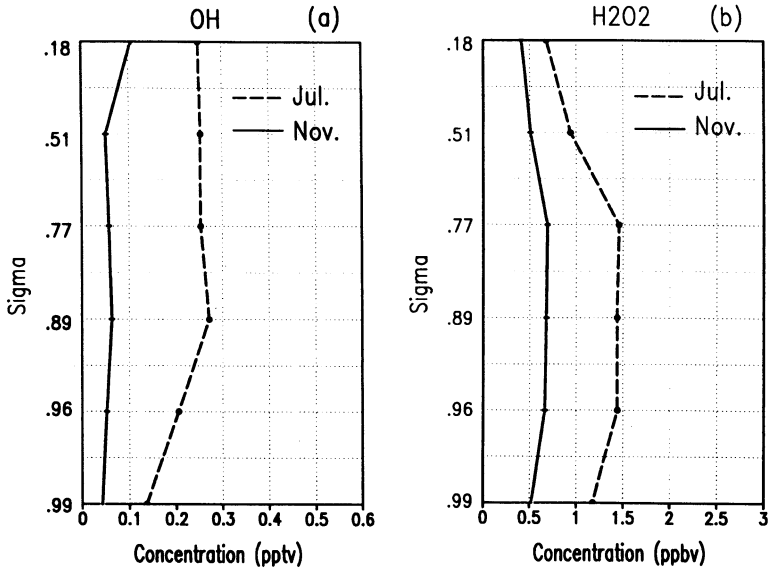

Fig. 1. Monthly and domain averaged vertical profiles of (a) OH and (b) H_2O_2 for July 1994 and November 1994. The data are from the simulation of Luo et al. (2000). Units are pptv for OH and ppbv for H_2O_2.

dimensional monthly mean values of H_2O_2 are taken from the RADM simulations of Luo et al. (2000), and examples of H_2O_2 averged vertical profiles for July and November are shown in Fig. 1b. Observations of H_2O_2 concentration profiles over Japan and Hong Kong are reported by Barth et al. (2000) and indicate that values simulated by Luo et al. (2000) over this region (Fig. 1b) are reasonable.

In order to calculate the aqueous phase conversion, the sulfur model requires knowledge of liquid water content. As described above, the model explicitly calculates resolvable scale cloud water, and if cloud water is present at a certain grid point, it is assumed that the full grid point is covered by clouds. In the presence of convective clouds the fractional cloud volume is equal to 0.3 and a cloud water content of 2 g m^{-3} is assumed throughout the whole depth of the cumulus cloud for the $SO_2 \rightarrow SO_4^{2-}$ conversion calculations (Giorgi and Chameides, 1986).

Sulfur emission is from the database of Streets and Waldhoff (1999), which is representative of 1995 emissions (Fig. 2). In the present experiments no seasonal variation of emission rate is included. The sulfur total emission is divided into surface emission, which occurs throughout the depth of the bottom model layer ($\sim$45 m), and large-point emission from high source (e.g., industry stacks), which is equally distributed between the second ($\sim$110 m depth) and third ($\sim$300 m depth) model layers above the surface. It is assumed that 98% (by mole) of the sulfur is emitted in the form of SO_2 and 2% in the form of SO_4^{2-}. Fig. 2 shows that the sulfur emission mostly occurs over East and South China with two areas of pronounced emission maxima over South-West China (Sichuan Basin) and over the coastal regions of East China.

2.3. *Experiment design*

In this study, we use the same model domain as in Giorgi et al. (1999) and Qian and Giorgi (1999). The domain (indicated for example by the light shaded region of Fig. 6) covers East Asia and adjacent ocean areas at a horizontal grid point spacing of 60 km, and the model includes 14 vertical levels extending to 100 mb. The period of analysis is from 1 June 1994, to 31 December 1994. This encompasses the first 7 months of the CHINA-MAP base case period (June 1994–August 1995, Giorgi et al., 1999) and spans cli-

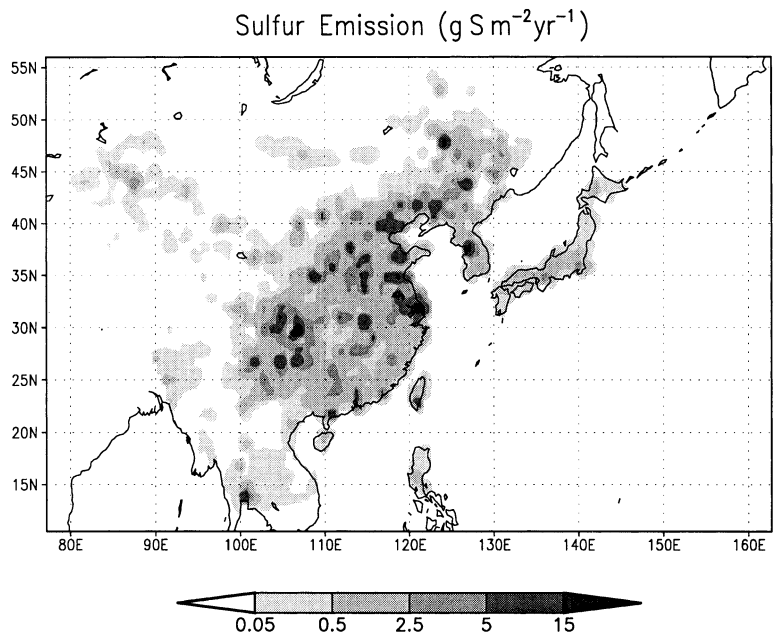

Fig. 2. Distribution of sulfur ($SO_2 + SO_4^{2-}$) emission over East Asia including both surface and high source (see text) (From Streets and Waldhoff 1999). Units are g S m^{-2} yr^{-1}.

matic conditions ranging from the wet summer monsoon season to the dry winter season. All simulations actually start on May 20 1994 and run continuously until 31 December 1994, with 0 initial values of SO_2 and SO_4^{2-} concentration. Qian and Giorgi (1999) show that it takes about 7–10 days for the sulfur model to equilibrate with the forcing meteorology, so that the first 10 days of the simulation are used as spin up for the sulfur model and are not included in the analysis.

Concerning lateral boundary conditions, we use the so called inflow/outflow boundary conditions, i.e., no sulfur is advected into the domain from outside and sulfur from the interior of the domain is freely advected out when it reaches the domain boundaries and the flow is outward. These assumptions neglect the contribution to the sulfur budget of sources outside the model domain, such as Europe, India and Southeast Asia. Due to the relatively short lifetime of sulfur compounds and to the magnitude of emissions over East Asia, this external contribution is small compared to the internal source (Roelofs et al., 2000).

Subsection 2.2 showed that the $SO_2 \rightarrow SO_4^{2-}$ conversion rate depends on various quantities that are not directly calculated by the current model, such as monthly averaged OH and H_2O_2 mixing ratios. In addition, the aqueous phase conversion rate depends on cloud properties, e.g., cloud liquid water content and fractional cover, that are characterized by a relatively high level of uncertainty (Giorgi et al., 1999). In order to assess the model sensitivity to these variables and the relative importance of emission, meteorological variables (e.g., cloud properties), and chemical and removal mechanisms, we designed the set of experiments described in Table 1. They can be grouped into the categories of sensitivity experiments to OH mixing ratio, H_2O_2 mixing ratio, cloud properties, SO_2 dry deposition velocity and sulfur emission.

An in depth analysis of the climatology of our simulation is already given by Giorgi et al. (1999). Basically, the model reproduced the seasonal cycle of circulation, precipitation and temperature over the region, with main problems being: A tendency to overestimate precipitation; simulation of a July southerly low level jet over East Asia of greater intensity than in the ECMWF analysis; a cold surface air temperature bias during the winter; a tendency to overestimate surface solar radiation and high level cloudiness. Giorgi et al. (1999) discuss the reasons for these problems and possible ways of improving them.

3. Results

3.1. Seasonal variability

Figs. 3a–f show the SO_2 and SO_4^{2-} column burden averaged over the whole interior of the domain for each simulated month and for the different groups of sensitivity experiments. The corresponding numerical values for July and November are reported in Table 2. These two months, also used in the previous study of Qian and Giorgi (1999), are representative of widely different climatic conditions over East Asia. July is in the middle of the summer monsoon season, with predominant low level southerly and southwesterly circulation and a maximum in precipitation and cloudiness. November is in the early stages of the dry season over East Asia, with prevailing westerlies in the mid and high latitudes, easterlies in the sub-tropical regions, and relatively dry conditions over China.

The first feature of relevance in Figs. 3a–f is that, while the SO_2 burden shows a pronounced seasonal cycle, with a late fall maximum and a summer minimum, the SO_4^{2-} burden does not show a strong seasonality, with only a weak minimum in late winter. The SO_2 seasonal cycle is not due to emission, which is constant throughout the year. An understanding of this result can be gained from the analysis of source, transport and removal terms in Figs. 4a, b and Table 3. For SO_2, the gas and aqueous conversion terms, as well as the wet removal term, are higher in summer than winter. This is due to the higher temperatures, OH and H_2O_2 amounts, cloud water content and precipitation during summer, and leads to higher concentrations of SO_2 and higher SO_2 dry deposition sink in winter than in summer. For SO_4^{2-}, the maximum summer source due to $SO_2 \rightarrow SO_4^{2-}$ conversion is compensated by a summer maximum in the wet removal term, so that SO_4^{2-} does not show a pronounced seasonality. This result is in contrast to that of Qian and Giorgi (1999) who used a constant SO_4^{2-} source and thus, by not capturing the seasonality of the $SO_2 \rightarrow SO_4^{2-}$ conversion, found larger SO_4^{2-} amounts in November than in July.

Overall, aqueous conversion is the dominant

Table 1. *List of experiments performed in this study*

Experiment	OH	H_2O_2	Clouds	Other
OHOFF	no	no limitation[a]	base[b]	
OHCON	constant monthly[c]	no limitation	base	
OHLATDC	3D diurnal monthly[d]	no limitation	base	
OHLATDC2	as OHLATDC but doubled	no limitation	base	
H2O2OFF	as OHLATDC	no	base	
H2O2CON	as OHLATDC	constant monthly[c]	base	
H2O2MON	as OHLATDC	3D monthly[e]	base	
H2O2HF	as OHLATDC	as H2O2MON but halved	base	
CLW2	as OHLATDC	no limitation	clw × 2	
CLWHF	as OHLATDC	no limitation	clw × 0.5	
CLDFRA	as OHLATDC	no limitation	clfr × 0.7	
SO2DEPA	as OHLATDC	no limitation	base	$v_{dep}^{SO_2} = 0.4$ cm s^{-1} over land[f] $v_{dep}^{SO_2} = 0.8$ cm s^{-1} over ocean
SO2DEPB	as OHLATDC	as H2O2MON	base	v_{dep} as SO2DEPA
SO2X2A	as OHLATDC	no limitation	base	SO_2, source doubled
SO2X2B	as OHLATDC	as H2O2MON	base	source as SO2X2A v_{dep} as SO2DEPA

clw is the cloud water content; clfr is the cloud fractional cover; v_{dep} is the deposition velocity with reference to the bottom model level. Monthly OH and H_2O_2 values are from the simulation of Luo et al. (2000).
[a]No H_2O_2 limitation means that there is always sufficient H_2O_2 to oxidize all local SO_2.
[b]clw and clfr calculated by the model as described in the text.
[c]Single average monthly value throughout the whole domain.
[d]Three-dimensional varying monthly values with a superimposed diurnal cycle consisting of 0 during nighttime and correspondingly increased values during daytime.
[e]Three-dimensional varying monthly values.
[f]In all other experiments $v_{dep}^{SO_2} = 0.8$ cm s^{-1} over land and $v_{dep}^{SO_2} = 0.4$ cm s^{-1} over ocean.

pathway of $SO_2 \rightarrow SO_4^{2-}$ chemical conversion both in summer and winter. Dry deposition is a dominant SO_2 removal mechanism compared to wet deposition, while for SO_4^{2-} wet removal is the dominant sink and dry deposition gives only a small contribution to the tracer budget.

The advection term out of the domain has a greater contribution to the mass budget for SO_4^{2-} than SO_2 throughout the simulation. This can be explained in terms of the vertical profiles of the two tracers. Figs. 5a, b show the interior domain averaged monthly SO_2 and SO_4^{2-} profiles throughout the H2O2MON experiment, which is representative of most experiments. The SO_2 concentration shows a sharp vertical gradient, with most SO_2 being trapped below the lower 1-2 km because of rapid gas phase and aqueous phase conversion to SO_4^{2-}. By comparison, the SO_4^{2-} concentration shows a much reduced vertical gradient, especially in the summer months when vertical mixing by both dry and wet convection is most pronounced. This is because the SO_4^{2-} source is not only at the surface but, following the SO_2 concentration profile, extends upward into the lower troposphere. As larger amounts of SO_4^{2-} reach the mid and high troposphere, they are engulfed in mid and high tropospheric circulations and they are more efficiently transported out of the domain region. Also, SO_4^{2-} is a secondary product which can be formed from SO_2 near the boundaries of the domain and then advected out.

3.1.1. Sensitivity to OH and H_2O_2 amounts. We now turn our attention to an analysis of the sensitivity of SO_2 and SO_4^{2-} amounts to OH and H_2O_2. We have already seen in the previous discussion that the aqueous conversion pathway is dominant throughout the simulations. During the summer this is because of the abundant cloud water produced by the monsoon circulations, while during the winter this is caused by the relatively low temperature and OH values. The

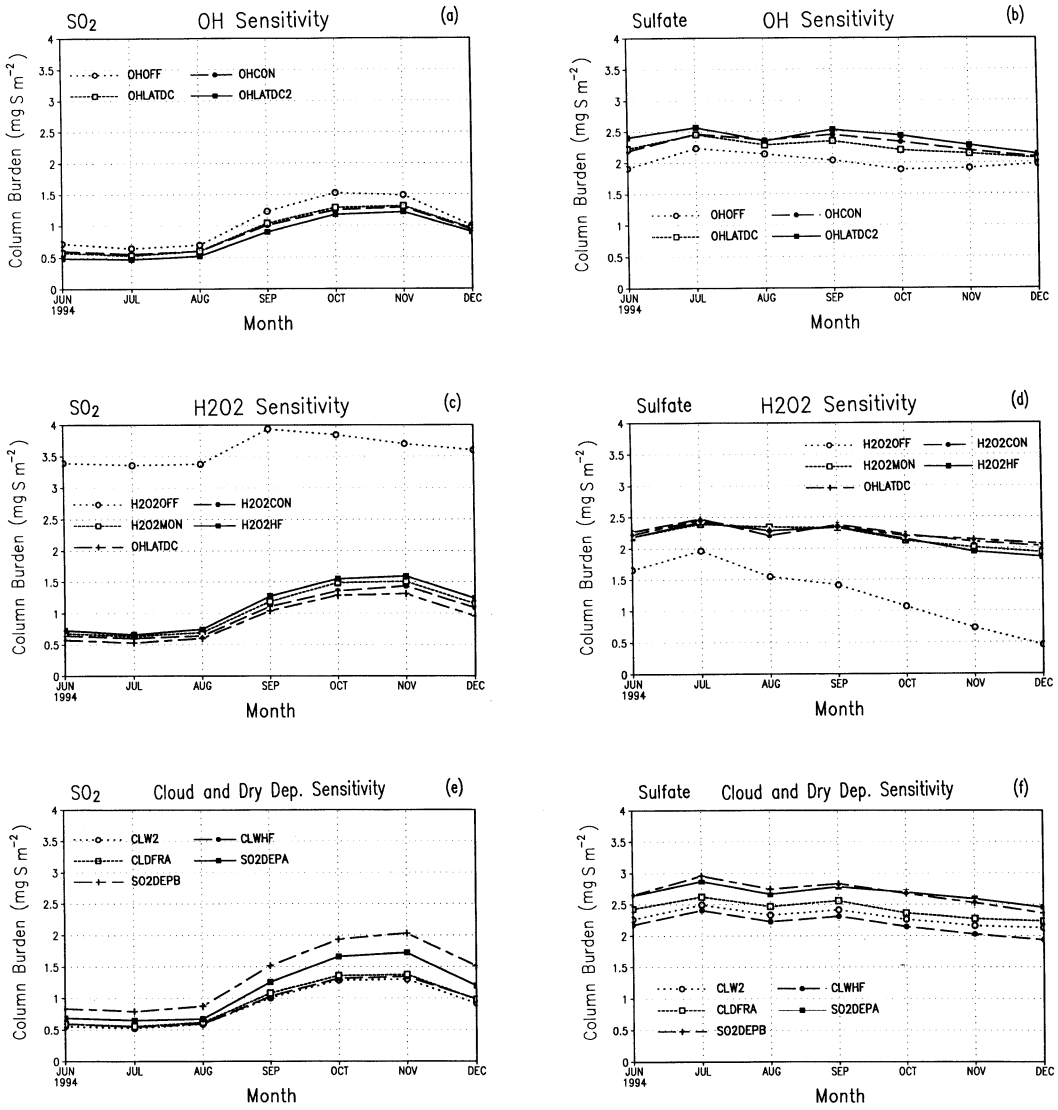

Fig. 3. Simulated monthly SO_2 and SO_4^{2-} column burdens averaged over the interior of the domain for the experiments in Table 1. (a) SO_2, OH sensitivity experiments; (b) SO_4^{2-}, OH sensitivity experiments; (c) SO_2, H_2O_2 sensitivity experiments; (d) SO_4^{2-}, H_2O_2 sensitivity experiments; (e) SO_2, cloud parameter and dry deposition sensitivity experiments; (f) SO_4^{2-}, cloud parameter and dry deposition sensitivity experiments. Units are mg S m^{-2}.

OH sensitivity experiments, for which it is assumed that the H_2O_2 concentration is not a limiting factor, show very small impact on SO_2 and SO_4^{2-} burdens by using constant vs. spatially and diurnally varying OH values, or by doubling the OH concentration. Removing altogether OH, i.e., short-circuiting the gaseous conversion pathway, leads to a reduction of the SO_4^{2-} amounts (and corresponding increase in SO_2 amounts) of 10% or less in November and December and 15–20% in the summer months.

Figs. 3c, d show the sensitivity of SO_2 and SO_4^{2-} column burden to the concentration of H_2O_2. First, comparison of Exp. OHLATDC with Exp. H2O2MON indicates that the assumption of no H_2O_2 limitation has a small effect, order of

Table 2. *Simulated SO_2 and SO_4^{2-} column burden averaged over the interior of the domain for July 1994 and November 1994 (Table1); units are mg S/m²*

Experiment	SO_2 July	SO_2 November	SO_4^{2-} July	SO_4^{2-} November
OHOFF	0.65	1.49	2.23	1.91
OHCON	0.55	1.29	2.46	2.19
OHLATDC	0.53	1.31	2.45	2.14
OHLATDC2	0.47	1.22	2.57	2.27
H2O2OFF	3.36	3.71	1.97	0.73
H2O2CON	0.60	1.44	2.47	2.10
H2O2MON	0.64	1.51	2.39	2.01
H2O2HF	0.66	1.60	2.42	1.94
CLW2	0.53	1.30	2.50	2.16
CLWHF	0.55	1.34	2.41	2.03
CLDFRA	0.56	1.38	2.62	2.27
SO2DEPA	0.65	1.73	2.87	2.59
SO2DEPB	0.80	2.03	2.96	2.52
SO2X2A	1.07	2.68	5.06	4.20
SO2X2B	1.67	4.27	5.79	4.83

10% or less, on the SO_2 and SO_4^{2-} burdens. Similarly, the use of uniform vs. spatially varying H_2O_2 concentration has essentially negligible effects. Removal of H_2O_2, i.e., short-circuiting of the aqueous phase conversion mechanism, has a large effect on both SO_2 and SO_4^{2-} column burden, with a marked seasonal dependency. In the winter, when gas phase conversion is minimum, the SO_4^{2-} burden is drastically reduced, by a factor of about 4 or more, and the SO_2 burden is substantially increased compared to the other experiments. The picture is different in the summer months. In the absence of H_2O_2, and in the presence of high OH concentration and high atmospheric temperatures, the gas phase conversion pathway attains its maximum efficiency, so that the SO_4^{2-} column burden is reduced only by about 25%, i.e., the gas phase pathway is efficient enough to substantially counterbalance the absence of the aqueous phase pathway.

Results from Exp. H2O2HF, in which the H_2O_2 concentration is halved with respect to the RADM-computed values, show little sensitivity compared to Exps. H2O2MON and OHLATDC (no H_2O_2 limitation). This indicates that, for our conditions, the transition between no-H_2O_2 and H_2O_2-unlimited regimes occurs rather abruptly at very low H_2O_2 concentration values. To examine this issue, we carried out an additional series of experiments in which the base H_2O_2 concentrations of Exp. H2O2MON were multiplied by increasingly small factors. The results showed that only when the H_2O_2 concentration is $\leqslant 5\%$ of the original monthly averaged values the sulfate amounts become sensitive to the value of H_2O_2 (not shown for brevity). Therefore, in most instances throughout the simulation the H_2O_2 concentration is higher than the SO_2 concentration.

It should be mentioned that in reality the H_2O_2 concentration is locally depleted in the sulfur oxidation process. In order to fully account for this effect, an additional prognostic equation for H_2O_2 should be used, which would add a significant level of complexity to our sulfur model. However, our results show that only for very strong depletion of H_2O_2 (in excess of 95%), the model becomes sensitive to the H_2O_2 concentration, and this does not likely occur often. Moreover, our H_2O_2 fields are taken from a full chemistry-transport model, so that the effect of H_2O_2 depletion by oxidation is at least approximately accounted for. For these reasons, the addition of an equation for H_2O_2 within the context of our region and experiment set up is not warranted at this stage of model development.

3.1.2. Sensitivity to cloud parameters and SO_2 dry deposition velocity. Figs. 3e, f and Table 2 show the sensitivity of the monthly averaged values of SO_2 and SO_4^{2-} column burden to cloud parameters. It can be seen that for both SO_2 and $SO_4^{2-}$the model sensitivity to the cloud liquid water content is not pronounced, less than 10%. This result is important in view of the difficulty of validating cloud water content in model simulations. The sensitivity to cloud fractional cover, another quantity of difficult evaluation, is somewhat greater, but still of order of 15% or less.

As mentioned, much uncertainty exists in the values of SO_2 dry deposition velocity, and the experiments SO2DEPA and SO2DEPB are designed to test the model sensitivity to this parameter. In these experiments, the value of v_{dep} is halved over land and doubled over ocean compared to Exps. OHLATDC and H2O2MON, respectively (Table 1). Results from these runs are reported in Tables 2, 3. Note that, because of the

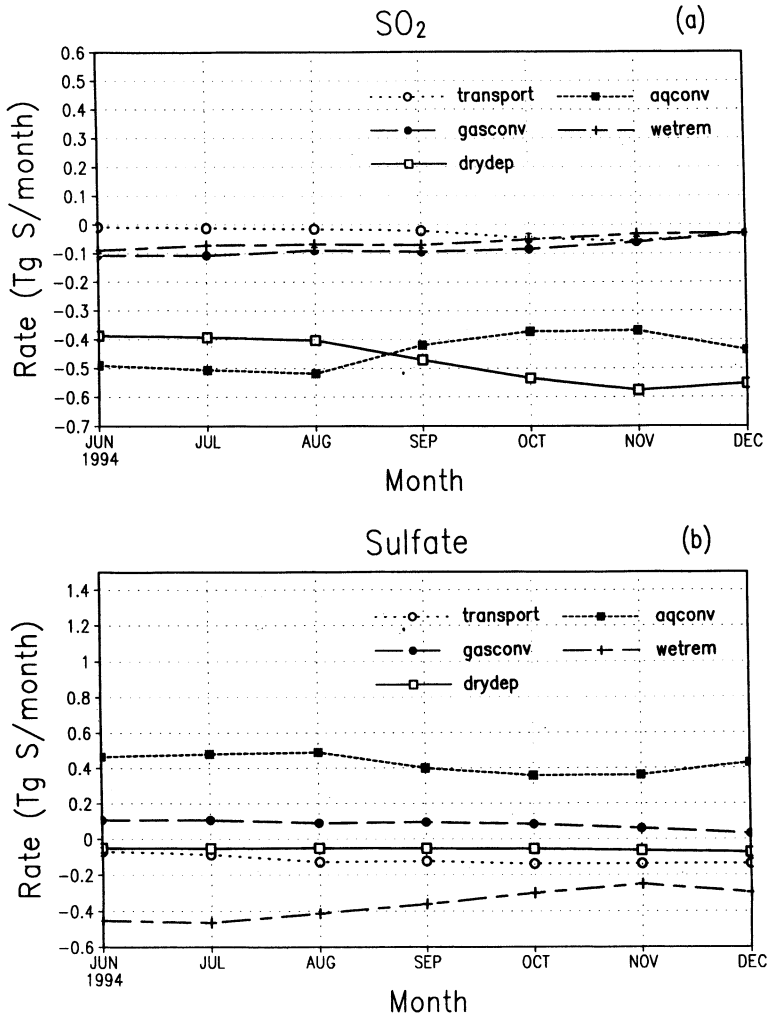

Fig. 4. Different components of the (a) SO_2 and (b) SO_4^{2-} budgets averaged over the interior of the domain for Exp. H2O2MON. Transport: transport across the domain boundaries; gasconv: gas phase conversion; aqconv: aqueous phase conversion; wetrem: wet removal; drydep: dry deposition. Negative (positive) values indicate loss (gain) of sulfur for the domain interior. Units are Tg S/month.

relatively short SO_2 lifetime, most SO_2 resides over land, and therefore the SO_2 column burden is most sensitive to the value of v_{dep} over land.

Table 3 shows that halving the value of v_{dep} over land (SO2DEPB) yields a decrease of the SO_2 dry deposition sink of 20–30%. This leads to an increase in SO_2 column burdens of 20–25% in the summer months and 30–35% in the fall and winter months, which in turn produces an increase in gas and aqueous phase conversion and an increase in SO_4^{2-} burden of 20–25%, similar in magnitude for the warm and cold months (Table 2). This shows that the sensitivity of the sulfur model to the SO_2 dry deposition velocity is significant, but it is substantially less than linear mostly because of the rapid chemical conversion of SO_2 to SO_4^{2-} and subsequent wet removal of SO_4^{2-}.

3.1.3. Comparison with observations and with previous work Very limited observations of sulfur compounds over East Asia are available. Some

Table 3. *Different components of the SO_2 and SO_4^{2-} budgets in July 1994 and November 1994 for a subset of experiments*

Experiment	Gas conversion	Aqueous conversion	Transport	Wet removal	Dry deposition
SO_2, July					
OHOFF	0.00	−0.60	−0.01	−0.11	−0.38
OHLATDC	−0.10	−0.54	−0.01	−0.10	−0.36
OHLATDC2	−0.16	−0.49	−0.01	−0.09	−0.35
H2O2OFF	−0.45	0.00	−0.12	0.00	−0.49
H2O2MON	−0.11	−0.51	−0.02	−0.08	−0.39
SO2DEPB	−0.14	−0.60	−0.02	−0.08	−0.27
SO_2, November					
OHOFF	0.00	−0.42	−0.06	−0.08	−0.55
OHLATDC	−0.06	−0.39	−0.05	−0.07	−0.53
OHLATDC2	−0.10	−0.36	−0.04	−0.07	−0.52
H2O2OFF	−0.13	0.00	−0.25	0.00	−0.69
H2O2MON	−0.06	−0.37	−0.06	−0.03	−0.58
SO2DEPB	−0.08	−0.46	−0.07	−0.04	−0.46
SO_4^{2-}, July					
OHOFF	0.00	0.57	−0.08	−0.45	−0.05
OHLATDC	0.09	0.51	−0.09	−0.47	−0.06
OHLATDC2	0.16	0.46	−0.10	−0.48	−0.07
H2O2OFF	0.44	0.00	−0.12	−0.30	−0.03
H2O2MON	0.11	0.48	−0.09	−0.46	−0.05
SO2DEPB	0.14	0.57	−0.10	−0.55	−0.06
SO_4^{2-}, November					
OHOFF	0.00	0.40	−0.13	−0.24	−0.07
OHLATDC	0.05	0.38	−0.14	−0.25	−0.08
OHLATDC2	0.10	0.35	−0.15	−0.25	−0.08
H2O2OFF	0.13	0.00	−0.06	−0.07	−0.03
H2O2MON	0.06	0.36	−0.14	−0.25	−0.06
SO2DEPB	0.08	0.45	−0.17	−0.32	−0.08

All quantities are averaged over the interior of the domain and "Transport" refers to advection across the domain boundaries. Negative (positive) values indicate loss (gain) of sulfur for the domain interior. Units are Tg S/Month. emission is 1.03 for SO_2 and 0.02 for SO_4^{2-}.

observation of sulfur wet deposition at some Chinese and Japanese sites are reported by Ichikawa and Fujita (1995) and Huang et al. (1995), but they refer to specific time periods different from the one used here. Barth et al. (2000) report observed profiles of SO_2 and SO_4^{2-} mixing ratio over Japan and Hong Kong. A large scatter is present in the observed data, but a number of features are evident: a pronounced near-surface maximum in both SO_2 and SO_4^{2-}; a sharp vertical decrease in mixing ratio in the lower troposphere; and a secondary maximum in the upper troposphere in the SO_2 profile. A qualitative comparison with these data indicates that our model results are generally in line with observations for SO_4^{2-}throughout the troposphere and for SO_2 in the lower troposphere. Our simulations do not produce the observed secondary SO_2 maximum in the upper troposphere, which may be an indication of relatively slow vertical transport, in

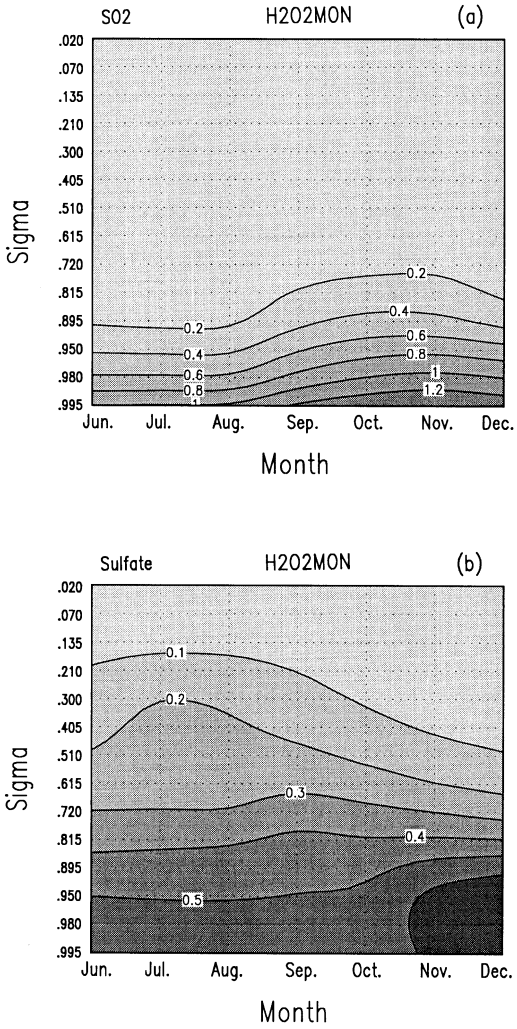

Fig. 5. Vertical profiles of (a) SO_2 and (b) SO_4^{2-} molar mixing ratio averaged over the interior of the domain as a function of month for Exp. H2O2MON. Units are ppbv.

particular by deep convective clouds. In our model we use a simple vertical mixing parameterization by cumulus clouds, without explicit calculation of the mass flux associated with deep convection. Note that the observations of Barth et al. (2000) do not suggest an upper tropospheric SO_4^{2-} maximum, perhaps because wet removal counterbalances the vertical transport by deep convection.

As part of the CHINA-MAP special observing period (September 1994 through August 1995), surface SO_2 observations were taken at three Chinese sites: Longfeng San (LF), located north of the Korean border; Qindao (QD), located on the coast of the Shandong peninsula; and Linan (LA), located on the Yantze river delta. A comparison of these point measurements with grid-box averaged model results is difficult due to the high horizontal variability of surface SO_2 and its dependence on emission. With this premise, Table 4 presents monthly averaged observations for the period September 1994–December 1994 and the corresponding simulated data (Exps. H2O2MON and SO2DEPB) at the grid points closest to the station locations. It can be seen that, although the model seemingly tends to overestimate SO_2 at LF and underestimate it at QD and LA, the model results are generally consistent with the observed values, with the experiment SO2DEPB giving a better agreement with observations.

Also important for model evaluation is the comparison with previous model results. Especially useful in this regard is the project COSAM recently organized to increase the understanding of the global distribution of sulfate aerosol via a comparison of large scale models of the sulfur cycle (Barrie et al., 2001). Ten General Circulation Models (GCMs) including the sulfur

Table 4. *Observed and simulated concentration of SO_2 during the period September 1994–December 1994 at 3 Chinese sites: Longfeng San (LF, 128°E, 44.5°N); Qindao (QD, 120.2°E, 36.1°N); Linan (LA, 119.5°E, 30.2°N)*

	Sept.	Oct.	Nov.	Dec.
LF				
observed	0.08	0.38	0.80	2.17
H2O2MON	0.60	1.44	2.27	2.42
SO2DEPB	1.04	2.34	3.70	4.30
QD				
observed	7.71	11.58	15.26	20.60
H2O2MON	6.55	7.31	7.63	9.37
SO2DEPB	8.39	9.40	10.01	12.31
LA				
observed	11.91	13.08	16.22	15.69
H2O2MON	2.55	5.20	5.18	6.77
SO2DEPB	4.21	7.98	8.28	10.87

The model data are at the grid point closest to the site's location. Units are ppbv.

cycle participated to the project, and of relevance for our work are the surface sulfur budget results presented by Roelofs et al. (2000) for the Southeast Asia region defined by 15–45°N and 105–140°E.

Table 5 shows column burden and budget terms for the Southeast Asia region in two of our experiments (H2O2MON and SO2DEPB) and in the 10 GCMs used in the COSAM exercise. Note that the COSAM values are for summer and winter months, while the RegCM values are for July and December 1994. For the COSAM GCMs both the range and average of the results are presented, as derived from the data reported by Roelofs et al. (2000). The SO_2 emission used in

Table 5. *SO_2 and SO_4^{2-} column burden and budget components simulated in two RegCM experiments and in the 10 GCM experiments of Roelofs et al. (2000) for the East asia region 15–45°N and 105–140°E*

	H2O2MON	SO2DEPB	10-GCM Range	10-GCM Ave.
SO_2	July 94	July 94	Summer	Summer
emission	2.66	2.66	2.26–2.98	2.61
gas conversion	−0.28 (−10%)	−0.35 (−13%)	−0.18–−0.83	−0.49 (−19%)
aqueous conversion	−1.23 (−47%)	−1.45 (−55%)	−0.41–−1.55	−1.10 (−42%)
dry deposition	−1.01 (−38%)	−0.70 (−26%)	−0.51–−1.28	−0.78 (−30%)
wet removal	−0.19 (−7%)	−0.20 (−8%)	0.0–−0.45	−0.11 (−4%)
transport from region	−0.03 (−1%)	−0.03 (−1%)	−0.29–0.98	−0.16 (−9%)
column burden	1.06	1.33	1.46–3.17	2.28
SO_2	Dec. 94	Dec. 94	Winter	Winter
emission	2.66	2.66	2.80–3.60	3.22
gas conversion	−0.16 (−6%)	−0.21 (−8%)	−0.08–−0.46	−0.30 (−9%)
aqueous conversion	−0.92 (−35%)	−1.15 (−43%)	−0.56–−1.59	−1.04 (−32%)
dry deposition	−1.48 (−56%)	−1.17 (−44%)	−1.39–−2.31	−1.78 (−55%)
wet removal	−0.08 (−3%)	−0.09 (−3%)	0.–−0.28	−0.06 (−2%)
transport from region	−0.14 (−5%)	−0.18 (−7%)	−0.18–0.41	−0.06 (−4%)
column burden	2.35	3.17	4.64–10.87	6.59
SO_4^{2-}	July 94	July 94	Summer	Summer
emission	0.06	0.06	0.–0.11	0.05
gas conversion	0.28 (18%)	0.35 (19%)	0.18–0.83	0.49 (30%)
aqueous conversion	1.23 (79%)	1.45 (78%)	0.41–1.55	1.10 (67%)
dry deposition	−0.13 (−9%)	−0.15 (−8%)	−0.07–−0.28	−0.16 (−9%)
wet removal	−1.19 (−76%)	−1.40 (−75%)	−0.34–−1.80	−1.29 (−76%)
transport from region	−0.22 (−14%)	−0.25 (−13%)	−0.39–0.64	−0.25 (−15%)
column burden	3.32	4.11	1.87–5.27	4.21
SO_4^{2-}	Dec. 94	Dec. 94	Winter	Winter
emission	0.06	0.06	0.–0.14	0.06
gas conversion	0.16 (14%)	0.21 (15%)	0.08–0.46	0.30 (22%)
aqueous conversion	0.92 (81%)	1.15 (81%)	0.56–1.59	1.03 (74%)
dry deposition	−0.17 (−15%)	−0.21 (−15%)	−0.08–−0.21	−0.17 (−13%)
wet removal	−0.64 (−57%)	−0.81 (−57%)	−0.59–−1.36	−0.87 (−64%)
transport from region	−0.36 (−31%)	−0.46 (−32%)	0.09–0.68	−0.32 (−24%)
column burden	2.79	3.50	1.76–6.17	3.47 5

Negative (positive) values indicate loss (gain) of sulfur for the region. For the 10 GCMs, the transport term is calculated as a residual to balance the budget due to the other terms, so that the average value is not necessarily consistent with the range. In parentheses are reported the % of the total positive or negative budget accounted for by each component. Units are mg S/m^2 for the column burden and mg S/(m^2 day) for the budget terms.

our simulations is close to that of the COSAM models during summer, but lower by about 25% in winter. This is because we did not assume a seasonality in the emission term. In addition, the COSAM models also included natural sulfur emission, for example due to DMS, which are estimated to contribute about 10% of the sulfur budget over industrialized regions (Rodhe, 1999).

Overall, the SO_4^{2-} column burden calculated by the RegCM is well within the COSAM GCM range, and in fact it is quite close to the GCM average. On the other hand, the SO_2 column burden simulated by the RegCM is lower than in the GCMs when using the high value of v_{dep} over land (H2O2MON) and close to the low end of the range when using the low v_{dep} value (SO2DEPB). This is suggestive of a relatively short SO_2 lifetime over the region in the RegCM experiments. We estimated the SO_2 lifetime as the ratio of column burden over removal and conversion rates and found an SO_2 lifetime of less than 1 day in summer and $\sim$1–1.5 days in late fall and winter. These lifetimes are dominated by aqueous phase $SO_2 \rightarrow SO_4^{2-}$ conversion. Factors that may contribute to the relatively low SO_2 values in the RegCM compared to the COSAM GCMs are the lower emission rates (especially in winter), the absence of natural sulfur sources and the possible advection of sulfur from regions outside of the model domain. In addition, the RegCM simulation refers to a specific and relatively wet year (Giorgi et al., 1994). From Table 5 it can be seen that the relative importance of the different SO_2 budget terms in the RegCM experiments is generally in line with that of the COSAM GCMs.

Regarding SO_4^{2-}, Table 5 shows that not only the column burden, but also the different components of the SO_4^{2-} budget and their relative importance within the budget are in good agreement with the COSAM GCMs. The RegCM values are all within the GCM range and quite close to the GCM average. This is not inconsistent with the relatively low SO_2 amounts, as the SO_4^{2-} cycle depends on the $SO_2 \rightarrow SO_4^{2-}$ conversion rate rather than the SO_2 concentration alone. The estimated lifetimes for SO_4^{2-} were 2.5–2.8 days for the summer months and 3.5 days for the winter months.

Finally, Tables 4 and 5 show that the results from experiment SO2DEPB are generally more in line with both observations and previous modeling studies. This suggests that the lower SO_2 deposition velocities over land used in experiment SO2DEPB may be more realistic than the estimates used by Luo et al. (2000).

3.2. *Spatial variability*

Figs. 6a–d show maps of the July and November SO_2 and SO_4^{2-} column burdens for the H2O2MON experiment. In July, the SO_2 column burden presents two sharp maxima, one over the Sichuan Basin and one over the central-eastern coastal regions of China. In addition, the July SO_2 column burden rapidly decreases away from the east China land areas. Comparison of the July SO_2 column burden with the source distribution of Fig. 2 indicates that the column burden is essentially tied to the emission distribution, a result which is easily understandable in view of the maximum efficiency of both gas and aqueous conversion pathways during the summer. In November, when the efficiency of conversion is reduced, synoptic scale transport horizontally mixes SO_2 and generates a more widespread distribution with a broad maximum extending from southwest to east China.

In general, the SO_4^{2-} column burden shows a smoother distribution than the SO_2 one, both in July and November. This is expected from the greater vertical and horizontal mixing discussed in Subsection 3.1. Especially in July, however, the SO_4^{2-} distribution shows distinct maxima over the Sichuan Basin and East China regions. The SO_4^{2-} distributions of Fig. 6 can be compared with those of Qian and Giorgi (1999), in which a spatially uniform SO_4^{2-} source was used. Although the simulations of Qian and Giorgi (1999) also produced maxima over these two regions, the maxima were much less marked than in the present experiments. This indicates that the distribution of SO_2 emission and subsequent conversion to SO_4^{2-}, along with regional meteorological factors, contribute to determine the spatial structure of SO_4^{2-} column burden.

Table 6 presents the correlation coefficient (r values) between monthly averaged SO_2 emission versus SO_2 column burden, SO_2 column burden versus SO_4^{2-} column burden, and SO_2 emission versus SO_4^{2-} column burden. The correlation is calculated for the experiment H2O2MON, but is representative of the general behavior of the

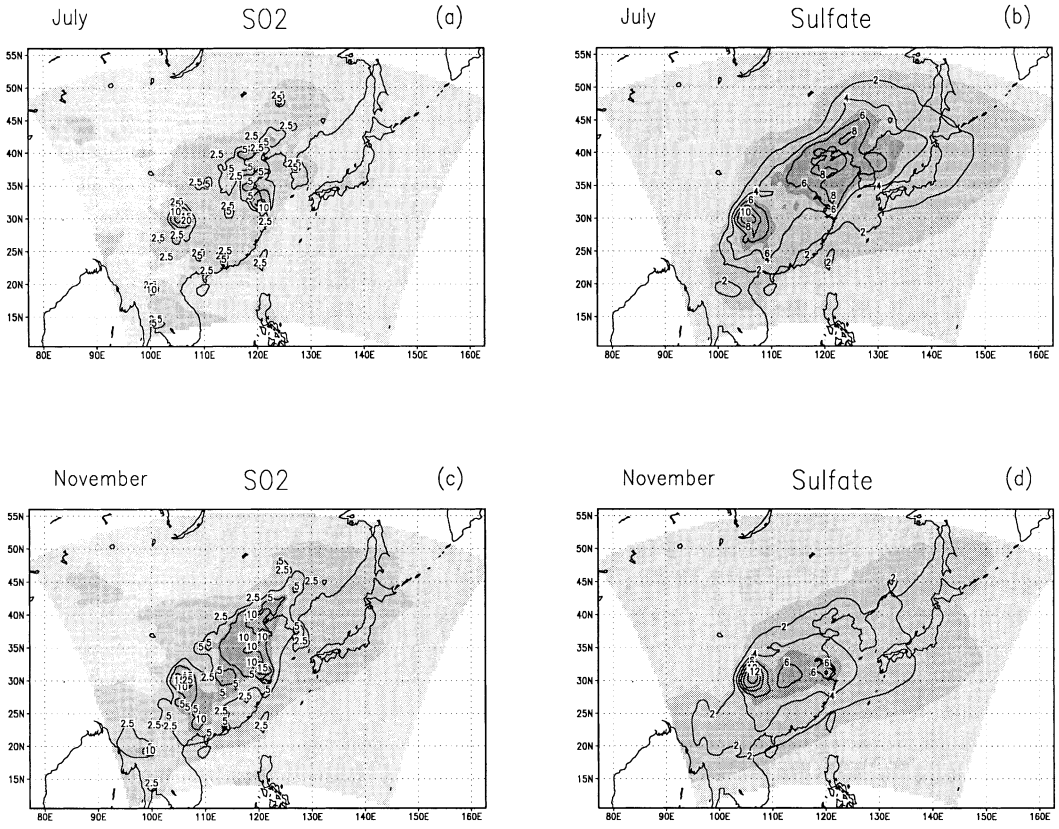

Fig. 6. Simulated SO_2 and SO_4^{2-} column burden for Exp. H2O2MON. (a) SO_2, July; (b) SO_4^{2-}, July; (c) SO_2, November; (d) SO_4^{2-}, November. The light shading indicates the model domain. Units are mg S m^{-2}.

Table 6. *Spatial correlation coefficient (r value) between SO_2 emission and SO_2 column burden; SO_2 column burden and SO_4^{2-} column burden; SO_2 emission and SO_4^{2-} column burden*

Month	SO_2 em. SO_2 bur.	SO_2 bur. SO_4^{2-} bur.	SO_2 em. SO_4^{2-} bur.
June	0.78	0.72	0.42
July	0.78	0.65	0.40
August	0.77	0.70	0.43
September	0.72	0.70	0.35
October	0.68	0.76	0.34
November	0.69	0.82	0.39
December	0.72	0.73	0.36
averaged	0.74	0.73	0.39

The experiment is H2O2MON.

model. It can be readily seen that high correlation is found between SO_2 emission and SO_2 column burden, explaining up to 60% of the spatial variability of SO_2. Also high is the correlation between SO_2 and SO_4^{2-} column burden, since the former acts as a source for the latter. Therefore, both for SO_2 and SO_4^{2-}, emission is the factor that explains the largest portion of the spatial variability structure. The correlation between SO_2 emission and SO_4^{2-} column burden is rather small, 0.425 or less. This implies that SO_2 emission cannot be used as an effective predictor for the spatial structure of SO_4^{2-} column burden, as chemical conversion, transport and removal processes effectively act to decouple the spatial structure of the two variables.

Figs. 7a, b show observed aerosol optical depths in the 0.75 μm wavelength for July and November averaged over the period 1979–1990 (Zhou et al.,

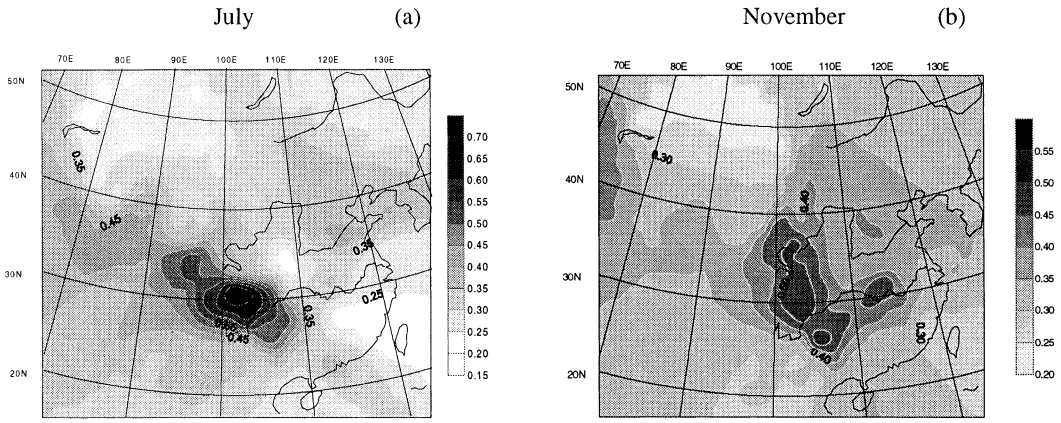

Fig. 7. Averaged observed aerosol optical depths over China for the period 1979–1990 including all aerosols. (a) July; (b) November. The data are from Zhou et al. (1998).

1998). The observed optical depth is due to all types of aerosols and refers to a different period than simulated, however it is a measure of observed aerosol amount and thus it allows an at least qualitative comparison with the simulated SO_4^{2-} spatial structure (Figs. 6b, d).

The model successfully reproduced the sharp aerosol maximum over the Sichuan Basin which, as mentioned, is due to a combination of high emission rates and relatively stagnant and humid local weather conditions. Air quality degradation and regional cooling induced by large aerosol loadings over the Sichuan Basin have raised substantial concern in recent years (Li et al., 1995; Qian et al., 1996). Figs. 6, 7 indicate that the model captured the areas of relatively large loadings over the Hua-bei region (including He-bei, Beijing, Bo-hai and the Korean peninsula) in July, and over the middle and low reaches of the Yangtze River in November. It is worth noting that these regional features are characterized by scales of a few hundred km or less and therefore are not well represented in present day global models. It is also evident that sulfate from anthropogenic origin cannot explain by itself the full aerosol optical depths observed over East Asia.

3.3. *Synoptic and daily variability*

Because transport and removal processes are dependent on atmospheric circulations, cloudiness, precipitation, and boundary layer processes, the SO_2 and SO_4^{2-} concentrations are likely to present substantial variability at sub-monthly temporal scales. Figs. 8a, b show the evolution of 3-h SO_2 and SO_4^{2-} column burden in Exp. H2O2MON averaged over the interior domain for the July and November periods. As expected, both SO_2 and SO_4^{2-} show variability at the diurnal scale and at temporal scales ranging from 2–3 days to 10 days. The former is clearly associated with the diurnal cycle of boundary layer and convective processes, and is most pronounced in July. The latter is associated with synoptic scale circulations, and is most pronounced in November.

Figs. 8a, b illustrate how the variability for SO_2 and SO_4^{2-} exhibits different features. In November the values of SO_2 are relatively high in the first two weeks of the month and then they drop significantly. By comparison, the sulfate averaged column burden is relatively constant throughout the entire month. The opposite behavior is found in July, when the SO_2 column burden is relatively stable throughout the month, while the sulfate concentration is low in the first 12 days, reaches a maximum in the central portion of the month and declines again significantly in the last 5 days.

To understand this behavior we need to look at the high temporal resolution characteristics of the $SO_2 \rightarrow SO_4^{2-}$ conversion, advective and removal terms. These are shown in Figs. 9a, d. All components of the budget exhibit a diurnal cycle, especially marked in July. For dry deposition this is related to the diurnal pulse of the boundary layer which induces a diurnal oscillation of vertical transport and, consequently, near-surface tracer

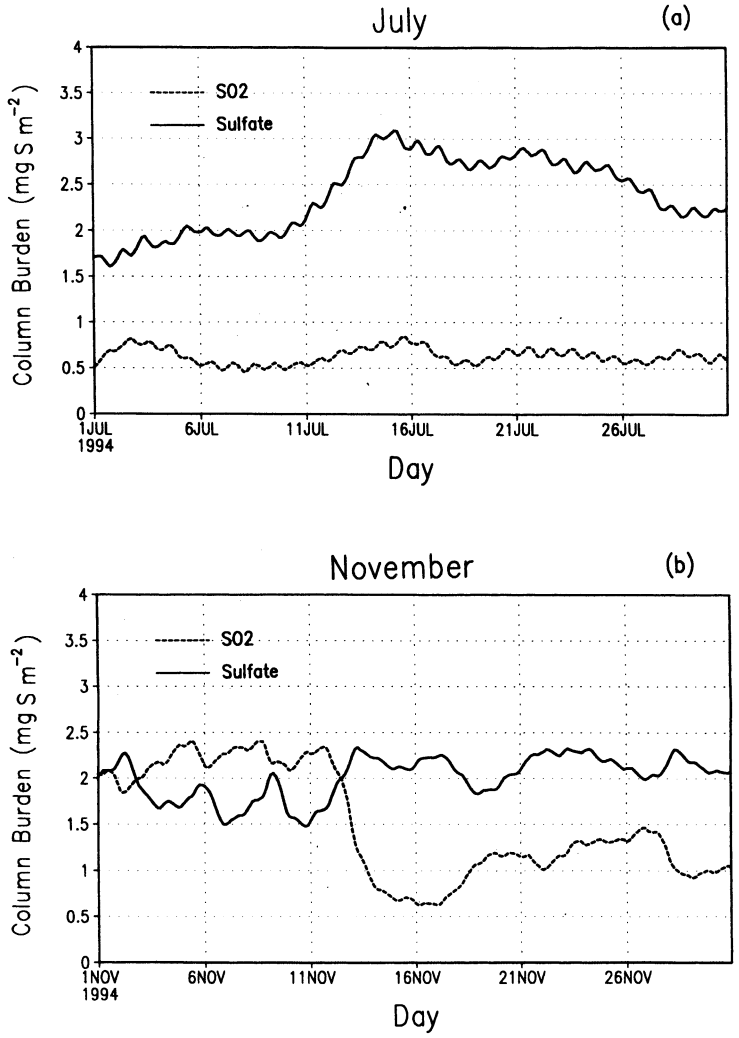

Fig. 8. Three-hourly values of SO_2 and SO_4^{2-} column burden averaged over the interior of the domain for Exp. H2O2MON. (a) July; (b) November. Units are mg S m^{-2}.

concentration. The diurnal oscillation of wet removal is mostly related to the diurnal pulse of moist convection generated by the Kuo-type cumulus scheme used in the present simulation (see also Giorgi et al., 1999). Moist convection affects not only the removal term but also the aqueous phase conversion term and the tracer vertical transport. Finally, the diurnal trend imposed to the OH concentration also contributes to the diurnal oscillation of the gas phase conversion term.

Variability at the 2–3 to 10 day scales is also evident in the removal and conversion terms, especially in November. The relatively high SO_2 concentration in the first 10 days of November is essentially caused by the low efficiency of aqueous phase conversion. For SO_4^{2-}, the aqueous phase conversion term is nearly balanced by the wet removal term, so that the SO_4^{2-} amounts are kept at a relatively constant level throughout the month. In July the SO_2 amounts remain relatively stable throughout the month because reduced aqueous phase conversion in cloud free conditions is counterbalanced by increased gas phase conver-

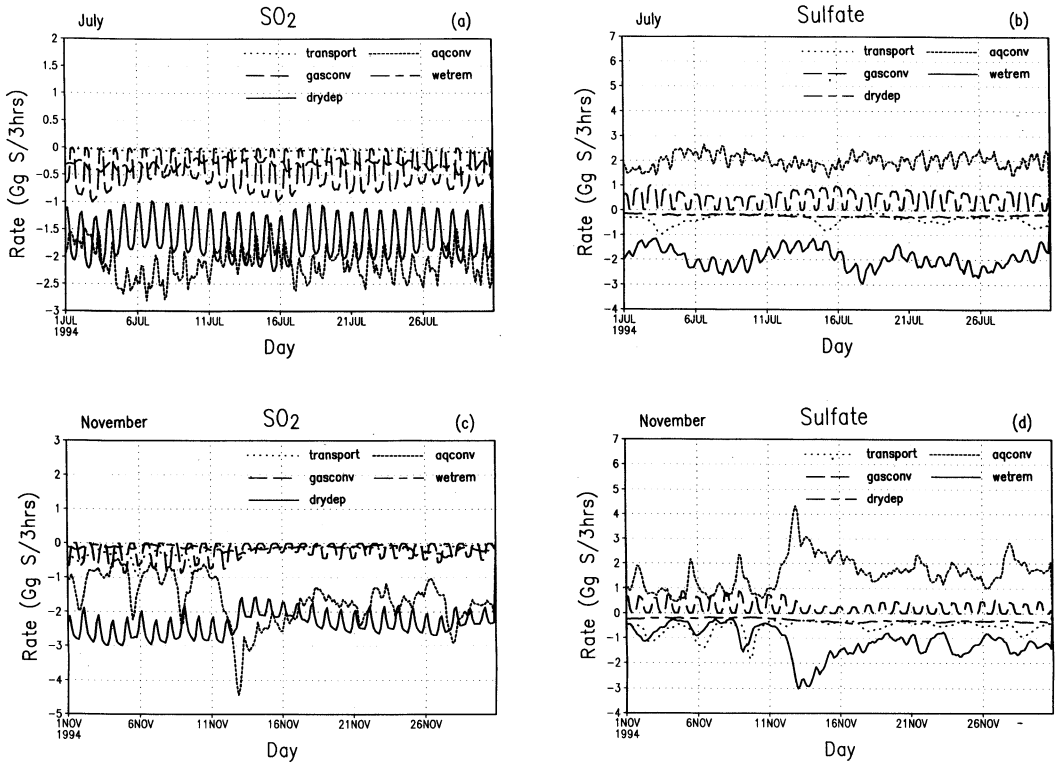

Fig. 9. Three-hourly values of the different components of the SO_2 and SO_4^{2-} budgets averaged over the interior of the domain for Exp. H2O2MON. (a) SO_2, July; (b) SO_4^{2-}, July; (c) SO_2, November; (d) SO_4^{2-}, November. Transport: transport across the domain boundaries; gasconv: gas phase conversion; aqconv: aqueous phase conversion; weterm: wet removal; drydep: dry deposition. Negative (positive) values indicate loss (gain) of sulfur for the domain interior. Units are Gg S/(3 h).

sion. Because of wet removal, the SO_4^{2-} amounts tend to be higher during cloud and precipitation free conditions (central part of the month) than during wet conditions. This discussion thus illustrates how the interplay of the gas and aqueous phase conversion mechanisms with the intermittent nature of the wet removal process cause different characteristics in the variability structure of SO_2 and SO_4^{2-} at the synoptic time scale..3cm

3.4. *Sensitivity to emission rate*

In Exps. SO2X2A and SO2X2B, we doubled the SO_2 emission rate within the model configuration of Exps. OHLATDC and SO2DEPB, respectively. The purpose of these experiments was to determine whether the model showed a non-linear response of sulfur amounts to emission within the present modeling framework. Also note that sulfur emission over East Asia is expected to double within the next decades (Streets and Waldhoff, 1999) so that these experiments might be representative of future emission scenarios. From Table 2 it can be seen that the response of the sulfur to doubling of emission is close to linear. This behavior can be explained by the fact that the model has little sensitivity to the assumed amounts of OH and H_2O_2 relative to the SO_2 concentration at the levels that these oxidants have for the present experiment. The removal processes seemingly do not add a strong element of non-linearity to the tracer model.

We should point out that in the present experiment the sulfate aerosol does not radiatively interact with the regional climate model, therefore in the presence of sufficient oxidant amounts a near

linear response is not surprising. However, the experiments of Qian and Giorgi (1999) show that when the aerosol radiative effects are included, processes such as cloud formation and precipitation, and thus aerosol removal and dispersion, are affected, possibly leading to feedback mechanisms.

4. Summary and conclusions

In this paper we discuss a series of experiments with a simplified anthropogenic sulfur model driven in on-line mode by a regional climate model over East Asia. Our main conclusions can be summarized as follows:

- The SO_2 and SO_4^{2-} column burdens showed significant variability at temporal scales from seasonal to synoptic and sub-daily. This is despite the use of a constant emission rate. The SO_2 and SO_4^{2-} column burdens showed different seasonal and synoptic scale behavior due to the interplay of chemical conversion, removal and transport processes.
- Both sulfur compounds, and especially SO_2, showed marked spatial variability. Because of its relatively short lifetime the SO_2 distribution is strongly tied to the emission distribution, and most of the SO_2 is confined to the lower troposphere. Conversely, SO_4^{2-} extends farther up into the mid and higher troposphere and it is more horizontally mixed by atmospheric circulations.
- Emission is the dominant term in regulating the SO_2 spatial distribution, and the sulfur amounts show a close to linear response to SO_2 emission. Aqueous phase conversion and wet removal are the primary factors that regulate the SO_4^{2-} amounts, with dry deposition and gas conversions playing secondary roles. Aqueous phase conversion and dry deposition are the dominant loss mechanism for SO_2.
- The model showed little sensitivity to variations in the OH concentration. The sensitivity to H_2O_2 concentration was greater, but only for very low levels of H_2O_2, less than 5% of the original values of Fig. 1b (i.e., 25–75 pptv). This implies that in most instances there was sufficient H_2O_2 for full oxidation of SO_2, a result that also minimizes the importance of neglecting oxidation by O_3.
- The sensitivity of SO_2 and SO_4^{2-} amounts to cloud fraction and liquid water content was less than 15%, while the sensitivity to different estimates of SO_2 dry deposition velocity was more pronounced, of the order of 20–30%.
- Overall, our results are in line with previous modeling studies and with very limited available observations, especially for SO_4^{2-}. Exp. SO2DEPB provides the best agreement with observations and previous work.

Although highly simplified, the present model appears capable to represent the first order processes involved with the anthropogenic sulfur cycle over East Asia. In particular, the model does not show a pronounced sensitivity to assumptions concerning OH and H_2O_2 concentration and cloud parameters, which is an encouraging indication of the model robustness. We are in the process of upgrading the parameterizations of direct and indirect aerosol effects of Qian and Giorgi (1999), and we plan to use the model to study possible regional climatic effects of sulfate aerosols of anthropogenic origin in multi year simulations for the East Asia region.

5. Acknowledgements

We thank Annica Ekman, Erik Kjellström, Henning Rodhe, Detlev Moller, Mary Barth, Deliang Chen, Congbin Fu and Xunqiang Bi for help and useful suggestions throughout the completion of this study. We also thank Yunfeng Luo for providing the observed optical depth data. This work was partially supported by the CHINAMAP project.

REFERENCES

Anthes, R. A. 1977. A cumulus parameterization scheme utilizing a one-dimensional cloud model. *Mon. Wea. Rev.* **105**, 270–286.

Anthes, R. A., Hsie, E. Y. and Kuo, Y. H. 1987. *Description of the Penn State /NCAR mesoscale model version 4 (MM4)*. NCAR technical note, NCAR/TN-282+STR.

Barrie, L. A., Yi, Y., Leaitch, W. R., Lohmann, U., Kasibhatla, P., Roelofs, G. J., Wilson, J., McGovern, F., Benkovitz, C., Melieres, M. A., Law, K., Prospero, J., Kritz, M., Bergmann, D., Bridgeman, C., Chin, M., Christensen, J., Easter, R., Feichter, J., Land, C., Jeuken, A., Kjellström, E., Koch, D. and Rasch, P. 2001. A comparison of large scale atmospheric sulfate

aerosol models (COSAM): Overview and highlights. *Tellus* **53B**, in press.

Barth, M. C., Rasch, P. J., Kiehl, J. T., Benkovitz C. M. and Schwartz, S. E. 2000. Sulfur chemistry in the National Center for Atmospheric Research Community Climate Model: Description, evaluation, features and sensitivity to aqueous chemistry. *J. Geophys. Res.* **105**, 1387–1415.

Chameides, W. L. 1984. The photochemistry of a remote marine stratiform cloud. *J. Geophys. Res.* **89**, 4739–4755.

Chameides, W. L. 1995. The Yangtze Delta of China as an evolving metro-agro-plex. *Proposal to the National Aeronautics and Space Administration*, Georgia Institute of Technology, Atlanta, Georgia, 80302, USA, 55 pp.

Chameides, W. C., Xingsheng, L., Xiaoyan, T., Xiuji, Z., Chao, L., Kiang, C. S., John, J. St., Saylor, R., Liu, S. C., Lam, K. S., Wang, T. and Giorgi, F. 1999. Is ozone pollution affecting crop yields in China?. *Geophys. Res. Letl.* **26**, 867–870.

Chin, M., Jacob, D. J., Gardner, G. M., Foreman-Fowler, M. S. and Spiro, P. A. 1996. A global three-dimensional model of tropospheric sulfate. *J. Geophys. Res.* **101**, 18,667–18,690.

DeMore, W. B., Sander, S. P., Golden, D. M., Hampson, R. F., Kurylo, M. J., Howard, C. J., Ravishankara, A. R., Kolb, C. E. and Molina, M. J. 1994. *Chemical kinetics and photochemical data for use in stratospheric modeling*. Jet Propulsion Laboratory Publ. 94–26.

Dickinson, R. E., Henderson-Sellers, A. and Kennedy, P. J. 1993. *Biosphere–aAtmosphere transfer scheme (BATS) version 1e as coupled to the NCAR community climate model*. Technical note, NCAR/TN-387 + STR, National Center for Atmospheric Research, Boulder, Colorado, 72 pp.

Feichter, J., Kjellström, E., Rodhe, H., Dentner, F., Lelieveld, J. and Roelofs, G. 1996. Simulation of the tropospheric sulfur cycle in a global climate climate. *Atmos. Environ.* **30**, 1693–1707.

Giorgi, F. 1995. Perspectives for regional earth system modeling. *Global and Planetary Change* **10**, 23–42.

Giorgi, F. 1989. Two-dimensional simulations of possible mesoscale effects of nuclear war fires. I: Model description. *J. Geophys. Res.* **94**, 1127–1144.

Giorgi, F. and Chameides, W. L. 1986. Rainout lifetimes of highly soluble aerosols and gases as inferred from simulations with a general circulation model. *J. Geophys. Res.* **91**, 14,367–14,376.

Giorgi, F. and Mearns, L. O. 1991. Approaches to regional climate change simulation: a review. *Rev. Geophys.* **29**, 191–216.

Giorgi, F. and Marinucci, M. R. 1996. An investigation of the sensitivity of simulated precipitation to model resolution and its implications for climate studies. *Mon. Wea. Rev.* **124**, 148–166.

Giorgi, F. and Mearns, L. O. 1999. Regional climate modeling revisited. An introduction to the special issue. *J. Geophys. Res.* **104**, 6335–6352.

Giorgi, F. and Shields, C. 1999. Tests of precipitation parameterizations available in the latest version of the ncar regional climate model (RegCM) over continental US. *J. Geophys. Res.* **104**, 6353–6375.

Giorgi, F., Marinucci, M. R. and Bates, G. T. 1993a. Development of a second generation regional climate model (RegCM2). Part I: Boundary-layer and radiative transfer processes. *Mon. Wea. Rev.* **121**, 2794–2813.

Giorgi, F., Marinucci, M. R., Bates, G. T. and De Canio, G. 1993b. Development of a second generation regional climate model (RegCM2). Part II: Convective processes and assimilation of lateral boundary conditions. *Mon. Wea. Rev.* **121**, 2814–2832.

Giorgi, F., Huang, Y., Nishizawa, K. and Fu, C. 1999. A seasonal cycle simulation over eastern Asia and its sensitivity to radiative transfer and surface processes. *J. Geophys. Res.* **104**, 6403–6423.

Grell, G. A., Dudhia, J. and Stauffer, D. R. 1994. *A description of the fifth generation Penn State/NCAR mesoscale model (MM5)*. NCAR technical note, NCAR/TN-398 + STR, 121 pp.

Holtslag, A. A. M., Bruijin, E. I. F. and Pan, H. L. 1990. A high resolution air mass transformation model for short-range weather forecasting. *Mon. Wea. Rev.* **118**, 1561–1575.

Huang, M., Wang, Z., He, D., Xu, H. and Zhou, L. 1995. Modeling studies on sulfur deposition and transport in East Asia. *Water Air Soil pollution* **85**, 1927–1932.

Ichikawa, Y. and Fujita, S. 1995. An analysis of wet deposition of sulfate using a trajectory model for East Asia, *Water Air Soil pollution* **85**, 1921–1926.

IPCC, 1996. *Climate change 1995: the science of climate change*, eds. Houghton, J. T., Meira Filho, L. G., Callander, B. A., Harris, N., Kattenberg, A. and Maskell, K. Cambridge University Press, Cambridge, UK, 572 pp.

Kasibhatla, P., Chameides, W. L. and John, J. St. 1997. A three-dimensional global model investigation of seasonal variation in the atmospheric burden of anthropogenic sulfate aerosols. *J. Geophys. Res.* **102**, 3737–3759.

Kiehl, J. T., Hack, J. J., Bonan, G. B., Boville, B. A., Briegleb, B. P., Williamson, D. L. and Rasch, P. J. 1996. *Description of the NCAR community climate model (CCM3)*. NCAR technical note, NCAR/TN-420 + STR, 152 pp.

Langner, J. and Rodhe, H. 1991. A global three-dimensional model of the tropospheric sulphur cycle. *J. Atmos. Chem.* **13**, 225–263.

Levine, S. Z. and Schwartz, S. E. 1982. In-cloud and below cloud scavenging of nitric acid vapor. *Atmos. Environ.* **16**, 1725–1734.

Li, X. W., Zhou, X. J. and Li, W. L. 1995. The cooling of Sichuan province in recent 40 years and its probable mechanism. *Acta Meteorologica Sinica* **9**, 57–68.

Lohmann, U., Salzen, K., McFarlane, N., Leighton, H. G. and Feichter, J. 1999. Tropospheric sulfur cycle in the Canadian general circulation model. *J. Geophys. Res.*, **104**, 26,833–26,858.

Luo C., John, J. St., Zhou, X. J., Lam, K. S., Wang, T. and Chameides, W. L. 2000. A nonurban ozone air pollution episode over eastern China: observations and model simulations. *J. Geophys. Res.* **105**, 1889–1908.

Pham, M., Muller, J. F., Brasseur, G. B., Granier, C. and Megie, G. 1995. A three-dimensional study of the tropospheric sulfur cycle. *J. Geophys. Res.* **100**, 26,061–26,092.

Qian, Y., Fu, C. B., Hu, R. M. and Wang, Z. F. 1996. Effects of industrial SO_2 emission on temperature variation in China and East Asia. *Climatic and Environmental Research* **2**, 143–149.

Qian, Y. and Fu, C. B. 1997. SO_2 emissions, sulphate aerosols and climate change. *Advances in Earth Science* **12**, 440–447.

Qian, Y. and Fu, C. B. 1998. *Composition and acidity of precipitation in China.* Proceedings of the 4th CAAP (Composition and acidity of Asian precipitation) Workshop, eds. H. Rodhe, J. Kuylenstierna, J. Boonjawat and G. Ayers, Bangkok, 9–12 November 1998, 99–104.

Qian, Y. and Giorgi, F. 1999. Interactive coupling of regional climate and sulfate aerosol models over eastern Asia. *J. Geophys. Res.* **104**, 6477–6499.

Rasch, P. J., Barth, M. C., Kiehl, J. T., Schwartz, S. E. and Benkovitz, C. M. 2000. A description of the global sulfur cycle and its controlling processes in the National Center for Atmospheric Research Community Climate Model, Version 3. *J. Geophys. Res.* **105**, 1367–1385.

Rodhe, H. 1999. Human impact on the atmospheric sulfur balance. *Tellus* **51A-B**, 110–122.

Roelofs, G. J., Kasibhatla, P., Barrie, L., Bergman, D., Bridgeman, C., Chin, M., Christensen, J., Easter, R., Feichter, J., Jeuken, A., Kjellström, E., Koch, D., Land, C., Lohmann, U., Rasch, P., Yi, Y. 2000. Analysis of regional budgets of sulfur species modelled for the COSAM exercise. *Tellus*, **53B**, in press.

Streets, D. G. and Waldhoff, S. T. 1999. Present and future emissions of air pollutants in China: SO_2, NO_x, and CO. *Atmos. Environ.* **34**, 361–372.

Wang, Z., Huang, M., He, D., Xu, H. and Zhou, L. 1996. Sulfur distribution and transport studies in East Asia using an Eulerian Model. *Advances in Atmospheric Sciences* **13**, 400–409.

Warneck, P. 1988. *Chemistry of the natural atmosphere.* Academic Press, San Diego, CA, 343 pp.

Zhou, X. J., Li, W. L. and Luo, Y. F. 1998. Numerical simulation of the aerosol radiative forcing and regional climate effect over China. *Scientia Atmospherica Sinica* **22**, 418–427.